AGU PUBLICATIONS

Geophysical Research Letters

RESEARCH LETTER
10.1002/2017GL076789

Key Points:
- We derive a relationship to predict turbulent vertical fluxes of passive tracers in the log layer
- The estimated fluxes from this relationship agreed well with those obtained directly with the typically applied eddy correlation method
- Turbulent fluxes can be estimated in more energetic flows and/or more tracers than previously possible

Correspondence to:
C. E. Bluteau,
cynthia.bluteau@uqar.ca

Citation:
Bluteau, C. E., Ivey, G. N., Donis, D., & McGinnis, D. F. (2018). Determining near-bottom fluxes of passive tracers in aquatic environments. *Geophysical Research Letters*, *45*, 2716–2725. https://doi.org/10.1002/2017GL076789

Received 12 DEC 2017
Accepted 15 FEB 2018
Accepted article online 20 FEB 2018
Published online 23 MAR 2018

Determining Near-Bottom Fluxes of Passive Tracers in Aquatic Environments

Cynthia E. Bluteau[1,2], Gregory N. Ivey[2], Daphne Donis[3], and Daniel F. McGinnis[3]

[1]Institut des sciences de la mer, Université du Quebec à Rimouski, Rimouski, Québec, Canada, [2]School of Civil, Environmental and Mining Engineering and the Oceans Institute, University of Western Australia, Crawley, Western Australia, Australia, [3]Aquatic Physics Group, Department F.-A. Forel for Environmental and Aquatic Sciences (DEFSE), Faculty of Science, University of Geneva, Geneva, Switzerland

Abstract In aquatic systems, the eddy correlation method (ECM) provides vertical flux measurements near the sediment-water interface. The ECM independently measures the turbulent vertical velocities w' and the turbulent tracer concentration c' at a high sampling rate (> 1 Hz) to obtain the vertical flux $\overline{w'c'}$ from their time-averaged covariance. This method requires identifying and resolving *all* the flow-dependent time (and length) scales contributing to $\overline{w'c'}$. With increasingly energetic flows, we demonstrate that the ECM's current technology precludes resolving the smallest flux-contributing scales. To avoid these difficulties, we show that for passive tracers such as dissolved oxygen, $\overline{w'c'}$ can be measured from estimates of two scalar quantities: the rate of turbulent kinetic energy dissipation ϵ and the rate of tracer variance dissipation χ_c. Applying this approach to both laboratory and field observations demonstrates that $\overline{w'c'}$ is well resolved by the new method and can provide flux estimates in more energetic flows where the ECM cannot be used.

1. Introduction

In aquatic environments such as rivers, lakes, estuaries, and ocean, mass transfers at the sediment-water interface (SWI) influence many biogeochemical processes and are also affected by the overlying turbulent flow. Examples include determining the flow conditions that enhance the release of pollutants from contaminated sediments (e.g., mining waste) or quantifying greenhouse gas exchanges from bottom sediments into waterways (e.g., Joyce & Jewell, 2003). Most exchange models are derived by measuring bulk transfers over time after disequilibrating the concentration between the sediment and the overlying water (Grant et al., 2012). The results are then related empirically to several nondimensional parameters characterizing the flow and sediments (e.g., O'Connor & Harvey, 2008). Only recently have turbulence and mean property measurements across the SWI enabled developing frameworks that characterize the interaction between aquatic flows and permeable sediments (e.g., Voermans et al., 2017). In aquatic systems, however, difficulties in measuring the vertical fluxes near the SWI have impeded advances in relating these turbulent exchanges with the overlying flow properties (see Grant & Marusic, 2011).

The eddy correlation method (ECM) has been adopted from the atmospheric sciences (see Foken et al., 2012) to obtain noninvasive and in situ flux measurements in aquatic environments. The ECM independently measures the turbulent vertical velocities w' and the turbulent tracer concentration c' at high sampling rates to obtain the vertical flux $\overline{w'c'}$ from their time-averaged covariance. This method requires identifying and resolving *all* the flow-dependent time (and length) scales contributing to $\overline{w'c'}$. These scales range from seconds to minutes in time and from millimeters to meters in length. Applying the ECM thus requires sensors that are sufficiently small and respond fast enough (< 1 s) to measure the smallest flux-contributing scales. With current technology, these small scales become increasingly difficult to resolve when the flow becomes more energetic (Figure 1a). Another difficulty is the need to correct for the physical separation between the two sensors (see Donis et al., 2015). A more significant challenge though is identifying an appropriate time-averaging window that includes the largest flux-contributing scales but excludes the nonturbulent motions (Lorrai et al., 2010; McGinnis et al., 2008). Because of these challenges, the ECM has had limited usage in aquatic systems, despite being used to examine dissolved oxygen (DO) fluxes (e.g., Lorrai et al., 2010), hydrogen sulfide (e.g., McGinnis et al., 2011), and temperature fluxes (e.g., Davis & Monismith, 2011).

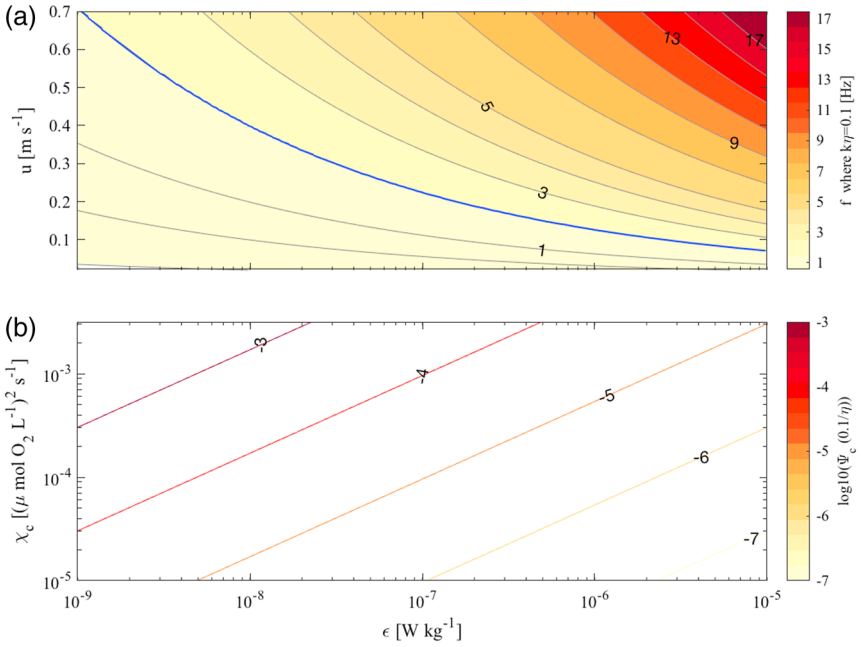

Figure 1. (a) The frequency corresponding to $k\eta$=0.1 as a function of ϵ and the mean flow speed u. The scales beyond this nondimensional wave number contribute less than 0.1% of the total flux $\overline{w'c'}$ according to the nondimensional cospectra for heat given by Kaimal et al. (1972). The thick blue line corresponds to the maximum usable frequency f_M of the DO sensor used in this study. Above this line, current technology cannot resolve most of the flux-contributing scales, precluding the use of the ECM to obtain $\overline{w'c'}$. DO sensors with slower response time limits the ECM to relatively quiescent environments. (b) Predicted energy of the concentration spectra $\Psi_c(k)$ at the high wave number limit of the inertial-convective subrange ($k\eta = 0.1$). When the measurement noise level in the observed spectra Φ_c exceeds $\Psi_c(0.1/\eta)$, lower wave numbers must be fitted to estimate χ_c.

To overcome the ECM's difficulties, we describe an alternative to estimate the vertical turbulent fluxes $\overline{w'c'}$ from measurements within the log-law region of the flow. The method applies to passive tracers that do not influence fluid density and so would exclude active tracers such as salinity and temperature. Our derived relationships enable quantifying $\overline{w'c'}$ more readily over a broader range of flow conditions and for potentially more tracers than currently possible with the ECM. Below, we first present the theory upon which our method is based on, followed by its application against controlled laboratory experiments and field observations.

2. Theory

Consider a steady, two-dimensional, parallel flow in the (x, z) plane over a hydraulically smooth bottom boundary. The mean velocity $u = u(z)$ does not vary in x, and u' and w' refer to the turbulent velocity components in the x and z directions, respectively. The turbulent kinetic energy equation reduces to a balance between the production of turbulent kinetic energy and the dissipation of turbulent kinetic energy ϵ (Tennekes & Lumley, 1972)

$$-\overline{u'w'}\frac{du}{dz} = \epsilon \tag{1}$$

where the mean velocity $u(z)$ profile is given by

$$\frac{u(z)}{u_*} = \frac{1}{\kappa}\ln z^+ + A \tag{2}$$

Here u_* denotes the friction velocity, $z^+ = u_* z/\nu$ is the nondimensional height above the bottom, ν is the viscosity of the fluid, and parameter A depends on bottom roughness. We set the von Kármán's constant κ for velocity to $\kappa = 0.39$ as revised by Marusic et al. (2013) using laboratory and atmospheric observations over a wide range of Reynolds number. Within the logarithmic region described by (2), the turbulent vertical momentum flux is equal to

$$-\overline{u'w'} = u_*^2 \tag{3}$$

Equations (1) to (3) can be simplified to

$$u_* = (\epsilon \kappa z)^{1/3} \tag{4}$$

The above relationship also apply to hydraulically rough bottom boundaries where the mean velocity profile is given by

$$\frac{u(z)}{u_*} = \frac{1}{\kappa} \ln\left(\frac{z}{z_o}\right) \tag{5}$$

where z_o is a length scale representative of the bottom roughness.

Consider now a passive tracer in the flow where $c = c(z)$. Analogous to (1), the tracer variance equation reduces to a balance between production of tracer variance and dissipation of tracer variance χ_c

$$-2\overline{w'c'}\frac{\mathrm{d}c}{\mathrm{d}z} = \chi_c \tag{6}$$

Following Pirozzoli et al. (2016), the mean tracer profile $c(z)$ is described by

$$\frac{c(z) - c_{\mathrm{SWI}}}{c_*} = \frac{1}{\kappa_c} \ln z^+ + B \tag{7}$$

where $\kappa_c \approx 0.46$ is the von Kármán constant for the tracer, c_{SWI} is the tracer concentration at the SWI, and B is a function of Schmidt number. Here the friction tracer concentration c_* is defined as

$$c_* = \frac{D}{u_*}\frac{\mathrm{d}c}{\mathrm{d}z}\Big|_{\mathrm{SWI}} \tag{8}$$

where D is the molecular diffusivity of the tracer (Pirozzoli et al., 2016). Analogous to (3), within the logarithmic region, the turbulent vertical tracer flux is

$$-\overline{w'c'} = u_* c_* \tag{9}$$

which from (6) and (8) yield

$$c_* = \left(\frac{\chi_c \kappa_c z}{2u_*}\right)^{1/2} \tag{10}$$

Finally, by substituting (4) and (10) into (9) we obtain

$$-\overline{w'c'} = u_* c_* = \sqrt{\frac{\kappa_c \kappa^{1/3}}{2}}\epsilon^{1/6}\chi_c^{1/2} z^{2/3} = 0.41\epsilon^{1/6}\chi_c^{1/2} z^{2/3} \tag{11}$$

demonstrating that in the log-law region, the vertical tracer flux $\overline{w'c'}$ can be estimated from measurement of two scalar quantities: the rate of turbulent kinetic energy dissipation ϵ and the rate of tracer variance dissipation χ_c, both measured at the same height z above the bottom.

We expect equation (11) to apply also for flows over hydraulically rough beds, provided both the velocity and scalar profiles are logarithmic above the viscous sublayer. Equation (11) shows that the predicted fluxes $\overline{w'c'}$ are independent of the roughness length z_o. For velocity, the vertical profile remains logarithmic for rough surfaces, even for very rough surfaces such as coral beds (Monismith, 2007). Few studies, however, have examined the mean and turbulence properties of a passive scalar over rough beds. Those that exist have focused on plume dispersion from single point release at a solid boundary (e.g., Rahman & Webster, 2005). These studies, nevertheless, suggest that the mean vertical concentration profile retains the same shape over both smooth and rough beds, although increased roughness leads to weaker concentration gradients as a result of increased mixing. This suggests that the concentration profile will remain logarithmic for rough surfaces, hence enabling fluxes to be estimated from (11).

Equation (11) also assumes that the SWI can be considered fluid dynamically impermeable and flow properties behave like those near a solid boundary. As Voermans et al. (2017) demonstrate, this is strictly true only when the permeability Reynolds number $Re_K = u_*\sqrt{K}/\nu \lesssim 0.01$, where K is the sediment permeability. This is the case for observations we describe below. For increasing Re_K, the SWI becomes increasingly permeable until

$Re_K > 1$ turbulent fluctuations actually start to penetrate below the SWI into the interstitial fluid (Voermans et al., 2017). As long as Re_K is small, however, the essential requirement in applying equation (11) is that a logarithmic layer exists and that both velocity and tracer are measured above the viscous layer within this logarithmic layer.

A logarithmic velocity profile of the form given in equation (2) is expected to exist for

$$3Re_*^{1/2} < z^+ < 0.15Re_* \tag{12}$$

(Marusic et al., 2013). The friction Reynolds number $Re_* = u_*\delta/\nu$ depends on the boundary layer thickness δ and the friction velocity u_*. In dimensional form, the outer limit of the logarithmic region z_M can be rewritten as $z_M = 0.15\delta$. There are various ways to determine the thickness δ from experimental data (see Marusic et al., 2013), and for our measurements below we apply a method similar to Metzger et al. (2007), based on the mean velocity profile, to determine whether our turbulence field measurements were within the logarithmic region. When a mean velocity profile is unavailable, we use the prediction $u \propto \epsilon^{1/3}$, applicable at a specific z above a rough bed, to gauge whether the measurements are within the logarithmic region. Over rough bottoms, the measurement height z must exceed the roughness length scale z_o, which can be a few centimeters over coral reefs (e.g., Monismith, 2007) but less than 1 mm over sandy (e.g., McGinnis et al., 2014) and gravel beds (e.g., Mignot et al., 2009). More precisely, laboratory results of near-boundary flows over large roughness elements (e.g., gravel beds) showed that the turbulent kinetic energy balance given by (1) is satisfied for $z \gtrsim 100z_o$ (Mignot et al., 2009). The instruments must thus measure above this threshold to estimate vertical fluxes $\overline{w'c'}$ from (11).

3. Data Sources and Analysis Procedures

3.1. Field Measurements

We applied the theory above to observations collected in the North Sea during a study on benthic oxygen exchanges (McGinnis et al., 2014; Rovelli et al., 2016). For this study, bottom landers were deployed in 74 m of water for about three tidal cycles (40 h) in August 2009 (56.502133°N, 3.002233°E) to characterize the mean and turbulence properties near the SWI. Before deploying the bottom landers, a shipboard conductivity, temperature, and depth (SBE9, Seabird) sampling at 24 Hz collected background temperature, salinity, dissolved oxygen, light transmission, and pH vertical profiles. The water column was well mixed over the bottom 35 m (see Figures 1b and 1c of McGinnis et al., 2014) with average temperatures of almost 7°C. For the purpose of assessing equation (11), we consider the water column to be unstratified over the vertical extent of the bottom landers.

Turbulence properties were measured with two bottom-mounted eddy correlation (EC) packages deployed at 0.08 and 0.12 m above the seabed (ASB). The EC consisted of a Nortek Vector velocity meter and a Clark-type oxygen microelectrode, both sampling at 64 Hz with their sensors separated by about 1 cm. The microelectrode's tip was 0.10 μm in diameter, while its 90% response time was less than 0.3 s, which translates to a time constant $\tau \approx 0.1$s and a maximum usable frequency of $f_M \lesssim 2$ Hz for the oxygen spectral observations (see below). The DO spectral observations were of higher quality closest to the seabed at 0.08 m ASB, and so we restrict our assessment to the measurements at this height.

Amongst the other instruments deployed, a 2 MHz downward looking Acoustic Doppler current profiler (AquaDopp; Nortek) measured velocities in high-resolution mode with 30 mm cells over the bottom 1.1 m. The AquaDopp collected 2,048 samples at 8 Hz every 15 min. Once quality controlled and time averaged, the AquaDopp measurements provided vertical background velocity profiles from 0.15 to 1.1 m ASB, which we used to estimate the boundary layer thickness δ.

During the 40 h deployment, the semidiurnal tide dominated the measured velocities at the site (McGinnis et al., 2014). From principal component analysis on the total velocities, water generally flowed at 45° from due east, essentially cross isobath—consistent with the major axis of the semidiurnal barotropic tidal ellipses at the site (Rovelli et al., 2016). The major axis of the total velocity ellipses were about 5 cm s^{-1} at the lowest EC instrument and increased to about 10 cm s^{-1} at 0.75 m above the seabed (not shown). Further off the seabed, the major axis reduced with increasing distance from the seabed, implying that the boundary layer thickness δ was likely less than 1 m.

Following Metzger et al. (2007), we define the boundary layer thickness δ as the height where the velocity gradient $\partial u/\partial z$ reaches its minimum value while satisfying the condition $\partial u/\partial z > 0$. These conditions essentially set δ to the height of maximum velocities over the vertical sampling range of the AquaDopp. These criteria yielded a median δ of about 0.9 m for our deployment—consistent with the δ derived from the vertical profile of the major axis of the velocity ellipses. From this δ, we estimate an outer limit for the logarithmic region z_M of about 0.13 m, that is, of the same order as the height of the furthest EC instrument from the seabed at 0.12 m ASB. These z_M estimates further justify using the estimates closest to the bottom to compare the vertical fluxes obtained from (11), denoted $\overline{w'c'}_{\mathrm{IDM}}$, against the ECM fluxes, denoted as $\overline{w'c'}_{\mathrm{ECM}}$.

Equation (11) requires that the flow properties near the SWI can be characterized as fluid dynamically impermeable. At the site, the bottom sediment was sandy with small ripples 0.5 cm high, and 2–3 cm long. Photos taken during the deployment showed there were no large roughness elements (McGinnis et al., 2014), while the estimated z_o was less than a few millimeters. The sediments' permeability, measured in the laboratory, was estimated to be $K = (6.6 \pm 0.1) \times 10^{-12}$ m^2, while ϵ ranged between 3×10^{-8} and 2×10^{-5} W kg^{-1} (McGinnis et al., 2014). These observations translate into permeability Reynolds number Re_K ranging from 0.002 to 0.02—within the range for which the flow properties are akin to those at an impermeable boundary (Voermans et al., 2017).

3.2. Laboratory Measurements

We also applied the above relationships to laboratory experiments that were part of a study designed to evaluate error sources of the ECM (see Donis et al., 2015). Their EC system differed from the field one only by the presence of a second DO sensor at 23 mm from the velocimeter's sampling volume. Here we use their velocity and DO time series from experiment 1a that lasted 210 min during which the DO sensors' orientation relative to the velocimeter was changed from upstream to downstream of the mean flow direction. Like the field EC system, the laboratory EC instrument sampled at 64 Hz with its sampling volume located 8 cm above the sediment. The total depth of water in the flume was 30 cm, and the mean flow speeds varied between about 3 and 8.4 cm s^{-1}. At each of the flow speeds examined, the velocities were steady for at least 30 min before changing the speed or the instrument orientation (see Figure 3 of Donis et al., 2015). The underlying sediments, collected from a mudflat in the Netherlands described by de Brouwer et al. (2000), were finer than the sand found at the North Sea field site. Therefore, the sediments' permeability K was likely smaller than the North Sea value of $K = 6.6 \times 10^{-12}$ m^2. Even with a permeability larger than this, the estimated Re_K would still be less than 0.01 given the flow properties in the flume. We thus consider the flow properties in the laboratory to be fluid dynamically impermeable.

To ascertain whether the velocities were measured within the logarithmic region described by (2), we use an alternative strategy to the field observations above. In channel flows the bottom layer thickness δ is typically set to half the total depth of water H (e.g., Marusic et al., 2013). For very permeable bottoms, experimental evidence suggests $\delta \approx H$ (Manes et al., 2011). With either criterion, the velocimeter's sampling volume was beyond the expected outer limit of the logarithmic region ($z_M \approx 2$–5 cm), but sampling at these heights is prohibitive with the EC system. Instead, we use the prediction $u \propto \epsilon^{1/3}$ to gauge whether our measurements were collected sufficiently close to the bottom. This test, although less stringent than the one in equation (12), has the advantage of not requiring independent measurements of the mean velocity profile $u(z)$. McGinnis et al. (2014) relied on this same relationship to identify when the bottom lander interfered with the velocity measurements, which we removed from our analysis herein. Its application to the laboratory measurements excluded data points when the EC instrument was oriented downstream; many of which were associated with slow advection velocities $u < 3$ cm s^{-1}, although it did exclude estimates later in the experiment around 155 min when $u \approx 7.4$ cm s^{-1}. This test did retain estimates associated with the highest u experimented in the laboratory.

3.3. Estimating $\overline{w'c'}$ With the ECM

The raw velocities were preprocessed and quality controlled prior to estimating $\overline{w'c'}_{\mathrm{ECM}}$. After discarding velocity measurements that were poorly correlated (< 70%), we box-car averaged the field measurements to 32 Hz and the laboratory measurements to 8 Hz. The velocities were then despiked using an acceleration threshold method (Goring & Nikora, 2002). Each spike was replaced by interpolating the neighboring data points. This process was repeated over the entire data set until the number

of replacements became negligible (<100 replacements for the field measurements). Data were rotated using a planar fit to avoid projecting horizontal fluxes (e.g., $\overline{u'c'}$) into the vertical fluxes $\overline{w'c'}_{ECM}$ (Lorke et al., 2013; Wilczak et al., 2001).

We extracted the DO fluxes with the SOHFEA processing software. The mean and fluctuating components of the vertical velocities and concentrations $w(t) = w + w'$ and $c(t) = c + c'$ were estimated by linear detrending (Moncrieff et al., 2004). The DO time series were time shifted relative to the velocities by a maximum of 2 s to account for the physical separation between its sensor tip and the acoustic Doppler velocimetry measurement volume ($\approx$ 1 cm) and second to account for the DO sensor's response time (Donis et al., 2015). We estimated the field fluxes over segment lengths, that is, time-averaging window, ranging from 10 to 60 s, which coincided with the time scales of the largest flux-contributing eddies (Lorrai et al., 2010; McGinnis et al., 2008). These fluxes were then box-car averaged onto the same 8.53 min long time segments used to estimate ϵ and χ_c below. For the laboratory fluxes, we used a 60 s time-averaging window and box-car averaged the fluxes onto the same time segments as our $\overline{w'c'}_{IDM}$ estimates.

One of the biggest challenge with applying the ECM, particularly at this site, was selecting an appropriate segment length to avoid including nonturbulent contributions in the vertical flux estimate (e.g., Lorrai et al., 2010; McGinnis et al., 2008, 2014). For a classical boundary layer flow, the time scale of the largest eddies are of the order of z/u_*, which translates to time scales of the order 10 to 100 s consistent with our chosen time-averaging window. With faster and more energetic flows, resolving all turbulent flux-contributing scales becomes even more challenging (Figure 1a) and would necessitate a more responsive DO sensor than currently available.

3.4. Estimating $\overline{w'c'}_{IDM}$ From ϵ and χ_c

To overcome the ECM's challenges, we propose using (11) to obtain $\overline{w'c'}_{IDM}$. This relationship relies on u_* and c_*, which we determine from ϵ and χ_c by fitting the observed turbulence spectra for velocity and passive scalar with their respective inertial subrange models. Using (11) has three main advantages over the ECM method. First, estimating ϵ and χ_c requires that the inertial subranges are sufficiently resolved for spectral fitting but, unlike the ECM, only a portion of these turbulence subranges must be resolved to estimate ϵ and χ_c and hence $\overline{w'c'}_{IDM}$. Second, the ECM's corrections and errors associated with the physical separation between the velocity and the scalar sampling volumes are avoided when using (11). Third, our proposed method is more readily applicable than the ECM as the flow becomes more energetic since the inertial subranges become increasingly broader.

3.4.1. Determining ϵ From the Velocity Spectrum

To obtain ϵ, and thus u_*, we fitted the velocity spectral observations $\Phi_{vj}(k)$ with its inertial subrange model $\Psi_{vj}(k)$:

$$\Psi_{vj}(k) = a_j C_k \epsilon^{2/3} k^{-5/3} \tag{13}$$

using the techniques described by Bluteau et al. (2011). Here k is the wave number expressed in rad m^{-1}, C_k is the empirical Kolmogorov universal constant that we set to $C_k = 1.5$ as per Sreenivasan (1995), and a_j is a constant dependent on the velocity component. In the vertical direction, $a_3 = 0.44$, which is 4/3 the value for the constant a_1 in the longitudinal direction (Pope, 2000).

We derived the velocity spectra from the velocity time series, which were preprocessed similar to the ECM. To avoid restricting the bandwidth for spectral fitting at low frequencies (wave numbers), we split the field time series into 512 s long segments that overlapped by 50% and the laboratory time series into 300 s long segments. The frequency spectra $\Phi_{vj}(f)$ were obtained by splitting further these segments into three subsets with a 50% overlap, which were Hanning windowed in the time domain before computing the fast Fourier transform. The resulting block-averaged spectra had more than 10 degrees of freedom. We invoked Taylor's frozen turbulence hypothesis to convert frequency spectral observations $\Phi_{vj}(f)$ into wave number spectra $\Phi_{vj}(k)$ via the mean flow speed u past the sensors.

3.4.2. Estimating χ_c From the Scalar Spectrum

To estimate χ_c, we use the same techniques developed for obtaining the dissipation of thermal variance from turbulence temperature spectra (Bluteau et al., 2017; Holleman et al., 2016). With ϵ already determined, χ_c

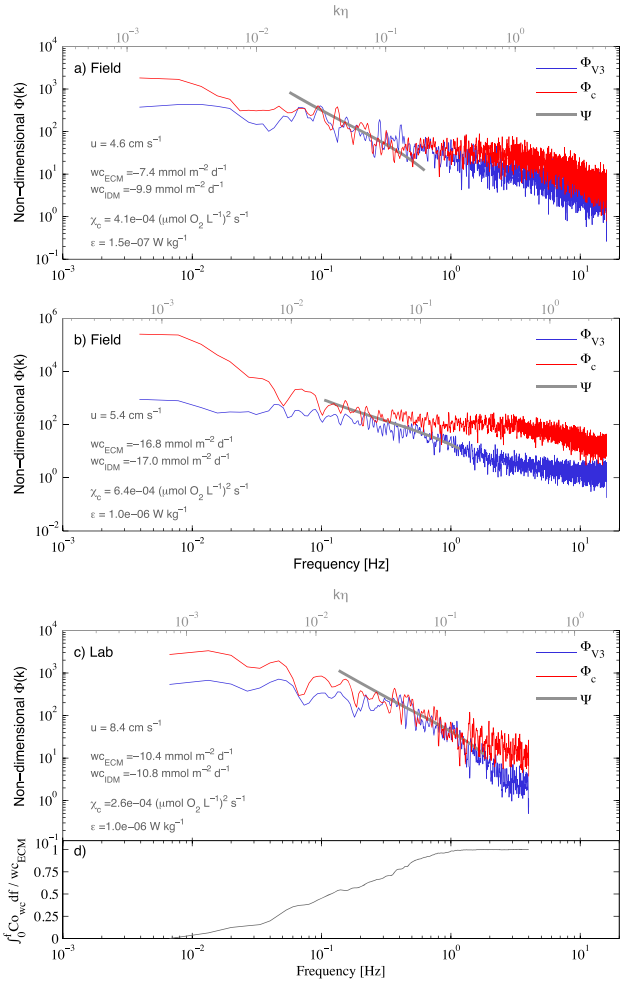

Figure 2. Example the vertical velocity spectra Φ_{V3} and for dissolved oxygen Φ_c spectra from the (a and b) field and the (c) laboratory measurements. (d) Cumulative integrated cospectrum of the vertical velocity and DO concentration for the example shown in Figure 2c. The cospectrum was nondimensionalized by the estimated flux $\overline{w'c'}_{ECM}$, while the velocity spectra by $(\epsilon\nu^5)^{1/4}$ and the DO spectra by $\chi_c\left(\frac{\epsilon^3}{\nu^5}\right)^{1/4}$. The secondary x axis are nondimensionalized by the Kolmogorov length scale $\eta = \left(\nu^3/\epsilon\right)^{1/4}$ to highlight the theoretical limit of the inertial subranges.

is then obtained by fitting the scalar spectral observations $\Phi_c(k)$ to the inertial-convective subrange model $\Psi_c(k)$ (Tennekes & Lumley, 1972):

$$\Psi_c(k) = C_o\chi_c\epsilon^{-1/3}k^{-5/3} \tag{14}$$

where we set the Obukhov-Corrsin universal constant to $C_o = 0.4$ (Sreenivasan, 1996). We obtained the spectral observations $\Phi_c(k)$ using the same averaging strategies as for velocity but, before fitting the inertial-convective model Ψ_c, we corrected the DO spectra $\Phi_c(f)$ for the sensor's time response $\tau \approx 0.1$s using a single-pole transfer function $H(f) = [1 + (2\pi\tau f)^2]^{-1}$ (e.g., Lorrai et al., 2010; McGinnis et al., 2008). We consider the spectra to be overcorrected when $H(f) > 3$, which translates to a maximum usable frequency $f_M = \frac{1}{\sqrt{2}\pi\tau} \approx 2$ Hz for our DO measurements. We note that the spectra may still be adversely impacted by the instrument's measurement noise for $f < f_M$.

The measurement noise must be less than the energy levels Ψ_c within the inertial-convective subrange to estimate χ_c. Figure 1b illustrates Ψ_c at $k\eta = 0.1$ as function of ϵ and χ_c where these energy levels correspond to the lowest predicted within the inertial-convective subrange. When the noise of the scalar measurements exceeds these levels, lower wave numbers within this subrange must be fitted to estimate χ_c. For constant energy (noise) levels, Figure 1b demonstrates that with decreasing ϵ, lower χ_c and therefore lower $\overline{w'c'}$ can be resolved by our method. The instrument noise also becomes less problematic for measurements collected further off the bed since ϵ decreases, while χ_c increases (see equations (4) and (10). With decreasing ϵ, the inertial-convective subrange also moves to lower k, further minimizing the impact of instrument noise when estimating χ_c from turbulence measurements in the log layer of the flow, justifying increasing the instruments' height off the bottom whenever feasible.

To exclude the high wave numbers k impacted by measurement noise and/or the low wave numbers k adversely impacted by the mean flow, we use the strategy evaluated by Bluteau et al. (2016) in the context of spectral fitting the inertial and/or viscous subranges of microstructure shear observations. We apply the mean absolute deviation (MAD) misfit criteria (equation (24) of Ruddick et al., 2000) to short subsets of the spectra of about half a decade long. If all subsets return a MAD$> 2(2/d)^{1/2}$, we completely discard the spectra (Ruddick et al., 2000). Otherwise, we set the final wave number range to estimate ϵ or χ_c to the subset that yielded the lowest MAD, provided the fitted k was within the theoretical wave numbers of the inertial subranges, that is, $k \lesssim 0.1/\eta$. The corresponding length scales are approximately an order of magnitude larger than the Kolmogorov length scale $\eta = \left(\nu^3/\epsilon\right)^{1/4}$.

4. Results and Assessment

We illustrate the advantages of equation (11) for estimating $\overline{w'c'}$ with example spectra and cospectra from the controlled laboratory experiments (Figure 2). Like the field examples in Figures 2a and 2b, the inertial-convective subranges are sufficiently resolved to obtain χ_c (Figure 2c), despite spectral energy attenuation at the highest frequencies because of the DO sensor's time response. The $\overline{w'c'}_{ECM}$ fluxes were in good agreement with the $\overline{w'c'}_{IDM}$ fluxes, even though the latter was derived by fitting only a portion of the observed Φ_{V3} and Φ_c spectra to obtain ϵ and χ_c, respectively. The cumulative integrated cospectra, on the other hand, show that obtaining $\overline{w'c'}_{ECM}$ relies on resolving a wider range of length (time) scales than $\overline{w'c'}_{IDM}$. More than 50% of the flux is contained at $k\eta \lesssim 0.01$, while the remainder is contained between $0.01 \lesssim k\eta \lesssim 0.1$ (Figure 2d). Resolving these turbulence scales was not problematic for either the laboratory or field measurements discussed here given the relatively low advection velocities ($u < 10$ cm s^{-1}). In faster and more

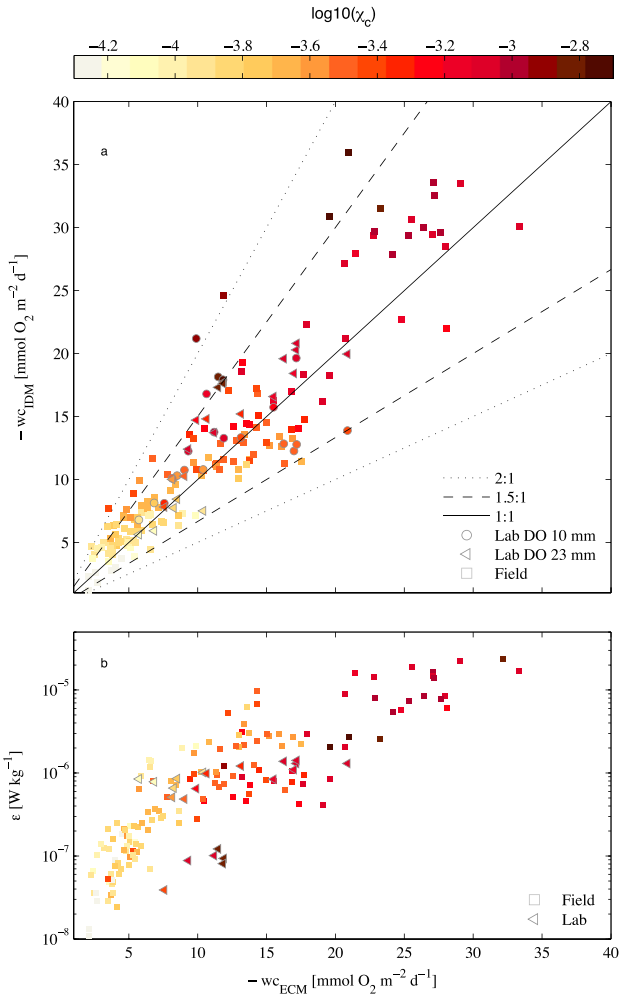

Figure 3. (a) Scatter of $\overline{w'c'}_{IDM}$, obtained via (11), plotted against $\overline{w'c'}_{ECM}$ for both the field and laboratory observations colored as a function of χ_c to illustrate the increase in $\overline{w'c'}$ with χ_c. (b) Scatter of the ϵ plotted against $\overline{w'c'}_{ECM}$. The large ϵ are associated with large mean advection speeds u.

energetic environments, however, the flux-contributing scales move to higher wave numbers (frequencies) and, given the time response of current DO sensors (Figure 1a), this then dramatically restricts using the ECM to estimate $\overline{w'c'}$. In these energetic situations, the inertial subranges become broader and more clearly defined, although instrument measurement may impede resolving low χ_c (Figure 1b). The vertical fluxes can nonetheless be determined more readily from (11), simplifying data processing and avoiding many challenges of the ECM such as correcting for the sensor separation and choosing an eddy-averaging window.

We compare the estimated vertical fluxes of oxygen $\overline{w'c'}_{IDM}$ from (11) against $\overline{w'c'}_{ECM}$ (Figure 3a). The majority (90%) of the $\overline{w'c'}_{IDM}$ estimates are within a factor of 1.5 of the ECM's. On average, $\overline{w'c'}_{IDM}$ were 10% larger than $\overline{w'c'}_{ECM}$. With increasing $\overline{w'c'}$, however, the $\overline{w'c'}_{IDM}$ estimates tended to be higher than those from the ECM (Figure 3a). We attribute this discrepancy to the loss of signal at high frequencies associated with the DO sensor's response time. With increasing flow speeds, Donis et al. (2015) demonstrated with the laboratory measurements presented here that the ECM progressively underestimates $\overline{w'c'}$ because the sensor's response time precludes resolving the flux-contributing scales at high frequencies. They found that this underestimation was 15% when $u > 0.07$ m s^{-1}, which is consistent with the tendency of our $\overline{w'c'}_{IDM}$ to exceed $\overline{w'c'}_{ECM}$ with increasing $\overline{w'c'}$ since the higher fluxes were associated with higher ϵ (Figure 3b) and faster flow speeds u (see Figure 3 of McGinnis et al., 2014). Our equation (11) thus represents a flexible approach to estimate $\overline{w'c'}$ at the SWI and is particularly useful in fast-moving flows when the ECM cannot resolve all the flux-contributing scales.

5. Conclusions

The theory presented in section 2 provides a practical alternative to the ECM for estimating turbulent vertical fluxes $\overline{w'c'}$ near the SWI. Our equation (11) relies on estimating the scalar quantities ϵ and χ_c from a portion of the inertial subranges of the velocity and scalar concentration spectral observations—enabling the flux to be determined when only part of the flux-contributing time and length scales are resolved. Challenges with implementing the ECM are also avoided, such as correcting for the physical separation between sensors and identifying the largest flux-contributing scales such that nonturbulent contributions are excluded from the estimated vertical flux.

Applying (11) requires the flow to be characterized as fluid dynamically impermeable (i.e., $Re_K \lesssim 0.01$) and to collect measurements within the logarithmic region. The latter criterion was respected for our field measurements and would also be satisfied for most coastal and marine environments given the sediments in these settings have permeabilities of the order of $K \approx 3 \times 10^{-11}$ m^2 (e.g., Wilson et al., 2008). Fluvial environments, however, can be more permeable and exhibit faster-moving flows—falling within the fully dynamically permeable regime ($Re_K > 1$). Care would be needed in applying (11) to predict $\overline{w'c'}$ in these situations. The extension of our approach to dynamically permeable flows is the subject of ongoing research.

For most coastal and marine environments, the approach here also suggests that $-\overline{w'c'}$ could be measured by estimating u_* and c_* from the measured vertical profiles of mean velocity $u(z)$ and of the mean scalar $c(z)$ above the SWI. This approach would significantly simplify the technological requirements of the scalar sensor regarding sampling frequency and response times. Vertical fluxes $-\overline{w'c'}$ could thus be quantified from measurements collected less frequently in time and enabling vertical fluxes to be quantified for not just dissolved oxygen but for any tracer where the mean concentration $c(z)$ can be measured.

Acknowledgments
C. E. B. thanks the University of Western Australia for awarding a Fay Gale Fellowship that instigated this research. C. E. B. also thanks the Natural Sciences and Engineering Research Council of Canada for funding a postdoctoral research fellowship to carry out the work. This project contributed to the research program of Québec-Océan. The Australian Research Council Discovery Projects (DP 140101322 and DP 180101736) also contributed funding. The data sets used in creating the figures are available in a repository (doi:10.5281/zenodo.1170757). The SOHFEA eddy correlation processing software is available at http://sohfea.dfmcginnis.com.

References

Bluteau, C. E., Jones, N. L., & Ivey, G. N. (2011). Estimating turbulent kinetic energy dissipation using the inertial subrange method in environmental flows. *Limnology and Oceanography: Methods*, *9*, 302–321. https://doi.org/10:4319/lom.2011.9.302

Bluteau, C. E., Jones, N. L., & Ivey, G. N. (2016). Estimating turbulent dissipation from microstructure shear measurements using maximum likelihood spectral fitting over the inertial and viscous subranges. *Journal of Atmospheric and Oceanic Technology*, *33*, 713–722.

Bluteau, C. E., Lueck, R. G., Ivey, G., Jones, N., Book, J., & Rice, A. (2017). Determining mixing rates from concurrent temperature and velocity measurements. *Journal of Atmospheric and Oceanic Technology*, *34*(10), 2283–2293. https://doi.org/10.1175/JTECH-D-16-0250.1

Davis, K. A., & Monismith, S. G. (2011). The modification of bottom boundary layer turbulence and mixing by internal waves shoaling on a barrier reef. *Journal of Physical Oceanography*, *41*(11), 2223–2241. https://doi.org/10.1175/2011JPO4344.1

de Brouwer, J., Bjelic, S., de Deckere, E., & Stal, L. (2000). Interplay between biology and sedimentology in a mudflat (Biezelingse Ham, Westerschelde, The Netherlands). *Continental Shelf Research*, *20*(10), 1159–1177. https://doi.org/10.1016/S0278-4343(00)00017-0

Donis, D., Holtappels, M., Noss, C., Cathalot, C., Hancke, K., Polsenaere, P., et al. (2015). An assessment of the precision and confidence of aquatic eddy correlation measurements. *Journal of Atmospheric and Oceanic Technology*, *32*(3), 642–655. https://doi.org/10.1175/JTECH-D-14-00089.1

Foken, T., Aubinet, M., & Leuning, R. (2012). The Eddy covariance method. In M. Aubinet, T. Vesala, & D. Papale (Eds.), *Eddy Covariance* (pp. 1–19). Dordrecht: Springer Atmospheric Sciences. Springer. https://doi.org/10.1007/978-94-007-2351-1_1

Goring, D. G., & Nikora, V. I. (2002). Despiking acoustic Doppler velocimeter data. *Journal of Hydraulic Engineering*, *128*(1), 117–126. https://doi.org/10.1061/(ASCE)0733-9429(2002)128:1(117)

Grant, S. B., & Marusic, I. (2011). Crossing turbulent boundaries: Interfacial flux in environmental flows. *Environmental Science & Technology*, *45*(17), 7107–7113. https://doi.org/10.1021/es201778s, pMID: 21793569.

Grant, S. B., Stewardson, M. J., & Marusic, I. (2012). Effective diffusivity and mass flux across the sediment-water interface in streams. *Water Resources Research*, *48*, W05548. https://doi.org/10.1029/2011WR011148

Holleman, R. C., Geyer, W. R., & Ralston, D. K. (2016). Stratified turbulence and mixing efficiency in a salt wedge estuary. *Journal of Physical Oceanography*, *46*(6), 1769–1783. https://doi.org/10.1175/JPO-D-15-0193.1

Joyce, J., & Jewell, P. W. (2003). Physical controls on methane ebullition from reservoirs and lakes. *Environmental and Engineering Geoscience*, *9*(2), 167–178. https://doi.org/10.2113/9.2.167

Kaimal, J. C., Wyngaard, J. C., Izumi, Y., & Coté, O. R. (1972). Spectral characteristics of surface-layer turbulence. *Quarterly Journal of the Royal Meteorological Society*, *98*(417), 563–589. https://doi.org/10.1002/qj. 49709841707

Lorke, A., McGinnis, D., & Maeck, A. (2013). Eddy-correlation measurements of benthic fluxes under complex flow conditions: Effects of coordinate transformations and averaging time scales. *Limnology and Oceanography: Methods*, *11*(8), 425–437. https://doi.org/10.4319/lom.2013.11.425

Lorrai, C., McGinnis, D. F., Berg, P., Brand, A., & Wüest, A. (2010). Application of oxygen eddy correlation in aquatic systems. *Journal of Atmospheric and Oceanic Technology*, *27*(9), 1821–1828. https://doi.org/10.1175/2010JTECHO723.1

Manes, C., Poggi, D., & Ridolfi, L. (2011). Turbulent boundary layers over permeable walls: Scaling and near-wall structure. *Journal of Fluid Mechanics*, *687*, 141–170. https://doi.org/10.1017/jfm.2011.329

Marusic, I., Monty, J. P., Hultmark, M., & Smits, A. J. (2013). On the logarithmic region in wall turbulence. *Journal of Fluid Mechanics*, *716*, R3. https://doi.org/10.1017/jfm.2012.511

McGinnis, D. F., Berg, P., Brand, A., Lorrai, C., Edmonds, T. J., & Wüest, A. (2008). Measurements of eddy correlation oxygen fluxes in shallow freshwaters: Towards routine applications and analysis. *Geophysical Research Letters*, *35*, L04403. https://doi.org/10.1029/2007GL032747

McGinnis, D. F., Cherednichenko, S., Sommer, S., Berg, P., Rovelli, L., Schwarz, R., et al. (2011). Simple, robust eddy correlation amplifier for aquatic dissolved oxygen and hydrogen sulfide flux measurements. *Limnology and Oceanography: Methods*, *9*(8), 340–347. https://doi.org/10.4319/lom.2011.9.340

McGinnis, D. F., Sommer, S., Lorke, A., Glud, R. N., & Linke, P. (2014). Quantifying tidally driven benthic oxygen exchange across permeable sediments: An aquatic eddy correlation study. *Journal of Geophysical Research: Oceans*, *119*, 6918–6932. https://doi.org/10.1002/2014JC010303

Metzger, M., McKeon, B., & Holmes, H. (2007). The near-neutral atmospheric surface layer: Turbulence and non-stationarity. *Philosophical Transactions of the Royal Society A*, *365*(1852), 859–876. https://doi.org/10.1098/rsta. 2006.1946

Mignot, E., Barthelemy, E., & Hurther, D. (2009). Double-averaging analysis and local flow characterization of near-bed turbulence in gravel-bed channel flows. *Journal of Fluid Mechanics*, *618*, 279–303. https://doi.org/10.1017/S0022112008004643

Moncrieff, J., Clement, R., Finnigan, J., & Meyers, T. (2004). Averaging, detrending, and filtering of eddy covariance time series. In Lee, X., Massman, W., & Law, B. (Eds.), *Handbook of micrometeorology* (Vol. 29, pp. 7–31). Atmospheric and Oceanographic Sciences Library. Dordrecht: Springer Netherlands. https://doi.org/10.1007/1-4020-2265-4_2

Monismith, S. G. (2007). Hydrodynamics of coral reefs. *Annual Review of Fluid Mechanics*, *39*, 37–55. https://doi.org/10.1146/annurev.fluid.38.050304.092125

O'Connor, B. L., & Harvey, J. W. (2008). Scaling hyporheic exchange and its influence on biogeochemical reactions in aquatic ecosystems. *Water Resources Research*, *44*, W12423. https://doi.org/10.1029/2008WR007160

Pirozzoli, S., Bernardini, M., & Orlandi, P. (2016). Passive scalars in turbulent channel flow at high Reynolds number. *Journal of Fluid Mechanics*, *788*, 614–639. https://doi.org/10.1017/jfm.2015.711

Pope, S. B. (2000). *Turbulent flows* (1st ed., p. 770). Cambridge, UK: Cambridge University Press.

Rahman, S., & Webster, D. (2005). The effect of bed roughness on scalar fluctuations in turbulent boundary layers. *Experiments in Fluids*, *38*, 372–384. https://doi.org/10.1007/s00348-004-0919-7

Rovelli, L., Dengler, M., Schmidt, M., Sommer, S., Linke, P., & McGinnis, D. F. (2016). Thermocline mixing and vertical oxygen fluxes in the stratified central North Sea. *Biogeosciences*, *13*(5), 1609–1620. https://doi.org/10.5194/bg-13-1609-2016

Ruddick, B., Anis, A., & Thompson, K. (2000). Maximum likelihood spectral fitting: The Batchelor spectrum. *Journal of Atmospheric and Oceanic Technology*, *17*(11), 1541–1555. https://doi.org/10.1175/1520-0426(2000)017<1541:MLSFTB>2.0.CO;2

Sreenivasan, K. R. (1995). On the universality of the Kolmogorov constant. *Physics of Fluids*, *7*(11), 2778–2784. https://doi.org/10.1063/1.868656

Sreenivasan, K. R. (1996). The passive scalar spectrum and the Obukhov-Corrsin constant. *Physics of Fluids*, *8*(1), 189–196.

Tennekes, H., & Lumley, J. L. (1972). *A first course in turbulence*. Cambridge, MA: MIT Press.

Voermans, J. J., Ghisalberti, M., & Ivey, G. N. (2017). The variation of flow and turbulence across the sediment-water interface. *Journal of Fluid Mechanics*, *824*, 413–437. https://doi.org/10.1017/jfm.2017.345

Wilczak, J. M., Oncley, S. P., & Stage, S. A. (2001). Sonic anemometer tilt correction algorithms. *Boundary-Layer Meteorology*, *99*(1), 127–150. https://doi.org/10.1023/A:1018966204465

Wilson, A. M., Huettel, M., & Klein, S. (2008). Grain size and depositional environment as predictors of permeability in coastal marine sands. *Estuarine, Coastal and Shelf Science*, *80*(1), 193–199. https://doi.org/10.1016/j.ecss.2008.06.011